

Semi-active control of ship mast vibrations using magneto-rheological dampers

Y.S. Cheng

Department of Naval Architecture and Ocean Engineering, Huazhong University of Science and Technology, Wuhan 430074, P.R. China

F.T.K. Au[†]

Department of Civil Engineering, The University of Hong Kong, Pokfulam Road, Hong Kong, P.R. China

J.P. Zhong

Department of Naval Architecture and Ocean Engineering, Huazhong University of Science and Technology, Wuhan 430074, P.R. China

(Received December 3, 2007, Accepted October 23, 2008)

Abstract. On marine vessels, delicate instruments such as navigation radars are normally mounted on ship masts. However the vibrations at the top of mast where the radar is mounted often cause serious deterioration in radar-tracking resolution. The most serious problem is caused by the rotational vibrations at the top of mast that may be due to wind loading, inertial loading from ship rolling and base excitations induced by the running propeller. This paper presents a method of semi-active vibration control using magneto-rheological (MR) dampers to reduce the rotational vibration of the mast. In the study, the classical optimal control algorithm, the independent modal space control algorithm and the double input – single output fuzzy control algorithm are employed for the vibration control. As the phenomenological model of an MR damper is highly nonlinear, which is difficult to analyse, a back-propagation neural network is trained to emulate the inverse dynamic characteristics of the MR damper in the analysis. The trained neural network gives the required voltage for each MR damper based on the displacement, velocity and control force of the MR damper quickly. Numerical simulations show that the proposed control methods can effectively suppress the rotational vibrations at the top of mast.

Keywords: magneto-rheological damper; neural network; semi-active control; ship mast; structural vibration.

1. Introduction

Slender masts are commonly used for mounting instruments such as navigation radars on ships due to their lightness and stiffness. However, the mast vibrations caused by wind loading, ship

[†] Ph.D., Corresponding author, E-mail: francis.au@hku.hk

rolling and base excitation induced by the running propellers often cause serious deterioration in radar-tracking resolution. To ensure satisfactory performance of the radar, the rotational vibrations particularly at the top of mast must be controlled within an allowable range stipulated by the relevant design standards. The vibration amplitudes of the mast with respect to the base may be reduced by stiffening the mast. This normally increases the weight of the mast on one hand, while it also increases the natural frequencies of the mast on the other hand, giving rise to higher accelerations and inertial forces. The inertial force cannot be eliminated easily either, since damping does not increase accordingly. Therefore more efficient vibration control methods are desirable. Such control methods will then be applicable not only to ship masts but also to masts with precision instruments installed on flexible structures like long-span bridges.

Hsueh and Lee (1992) employed an active control strategy to reduce the vibration of a ship mast. In their studies, the vibration control of the mast under wind loading and ship rolling were considered and good control effects were reported. However, apart from being expensive, an active control system relies greatly on external power and it may even destabilize the structural system.

Among various control systems investigated, namely passive control, active control, hybrid control and semi-active systems, the semi-active control system appears to be particularly promising Housner *et al.* (1997). A semi-active system does not inject mechanical energy into the controlled structural system that comprises the structure and the control devices, but it can be controlled to optimally reduce the dynamic response of the system. Hence in contrast to active control devices, semi-active control devices do not have the risk of destabilizing the structural system. It consumes less power and is fail-safe. In addition, studies have shown that a proper semi-active control system can perform significantly better than passive devices. It also has the potential to achieve most of the performance objectives of fully active systems, possibly providing effective response reduction under wind loading.

Friction dampers, viscoelastic dampers, viscous fluid dampers, tuned mass dampers, tuned liquid dampers and so on are primary energy dissipation devices applied to vibration control of engineering structures. Among these dampers, magneto-rheological (MR) dampers have obvious advantages over other dampers. MR dampers typically consist of a hydraulic cylinder containing micron-sized, magnetically polarizable particles suspended in a fluid that is usually a kind of oil. The behaviour of an MR fluid can be controlled by subjecting it to a magnetic field. The MR fluid flows freely in the absence of any magnetic field, but it behaves as a semi-solid under a magnetic field. Compared with other dampers, MR dampers consume less power. They are also relatively inexpensive, reliable and fail-safe.

Spencer *et al.* (1996) put forward a phenomenological model for MR dampers based on the Bouc-Wen hysteresis model to emulate their dynamic behaviour. Taking displacement, velocity and voltage as input, the model can predict the damper forces quite accurately. Unfortunately, because of the nonlinear characteristics of MR dampers, a similar model for the inverse dynamics appears difficult to obtain.

An alternative representation of MR dampers using neural networks was developed by Chang and Roschke (1999). A multi-layer perceptron neural network with six input neurons, one output neuron and twelve neurons in the hidden layer was used to simulate the dynamic behaviour of an MR damper. In some control applications, it is desirable for the damper to produce control forces based on some optimal control algorithms. In such cases, it is desirable to develop an inverse dynamic model that estimates the required input voltage for the damper to produce the necessary damper force. Chang and Zhou (2002) described the use of neural network to emulate the inverse dynamics

of MR dampers.

MR dampers have also been employed for seismic response control Dyke *et al.* 1996, Jansen and Dyke (2000), Xu *et al.* (2000), Jung *et al.* (2003). However, the application of MR dampers to the control of wind-induced structural vibrations has not been extensively elaborated by Zhu *et al.* (2004) and Wang *et al.* (2005) and little work on vibration control of ship masts using MR dampers has been reported.

The purpose of the study is to evaluate the effectiveness of MR dampers in reducing the adverse effects of ship mast vibrations due to wind loading, ship rolling and base excitation simultaneously. The control algorithms studied to provide desirable control forces by MR dampers include the classical optimal control algorithm by Bryson and Ho (1975), independent modal space control algorithm by Meirovitch (1985) and fuzzy control algorithm by Mamdani (1974) and Mohammed *et al.* (2004). A neural network is trained to give the required input voltage to the damper. Numerical simulations demonstrate that the proposed control method can effectively suppress the rotational vibrations at the top of mast.

2. Computational model of a ship mast

Fig. 1 shows a schematic diagram of a ship mast with navigation radar equipment mounted at the top. To facilitate vibration control using MR dampers, the mast is guyed by two pairs of cables which comprise a pair in the transverse plane and the other in the longitudinal plane. Each cable has one end connected to a stiff cross bar at the upper part of the mast and another end connected to one end of the shaft of an MR damper through a roller as shown in Fig. 2. Within each plane, the loop comprising the pair of cables and the shaft of the MR damper is pretensioned to an initial tension P_0 and the loop is assumed to be light and inextensible. Imagine that for whatever loading applied, the mast moves towards the right. The horizontal cable segment will move to the left inducing a damping force of f towards the right. If the damper is close to the mast, considering compatibility of the cable, one may conclude that the forces carried by the left and right cable

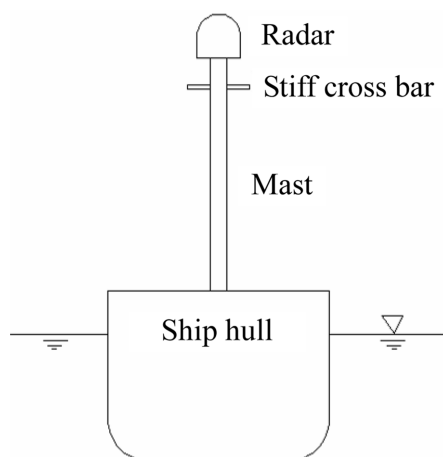


Fig. 1 Schematic diagram of the ship mast

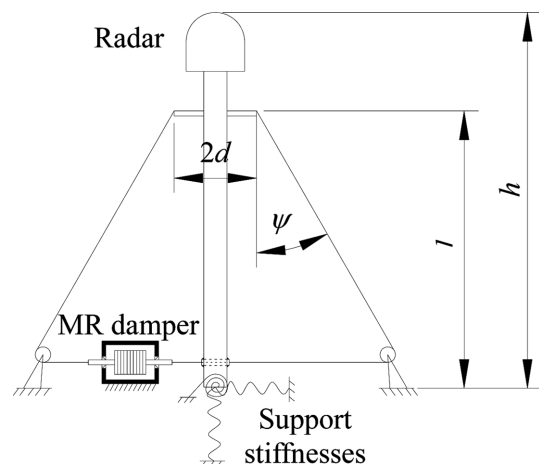


Fig. 2 Schematic diagram of the ship mast model in a typical cable plane

segments will be $(P_0 + 0.5f)$ and $(P_0 - 0.5f)$ respectively. The imperfect fixity of the mast at deck level is simulated by five springs to account for the flexibility of the deck, which comprise a vertical spring, and a horizontal spring and a rotational spring in each of the cable planes. Compared with the complete fixity assumption adopted by Hsueh and Lee (1992), the assumption of elastic support at the mast base is more realistic as the deck is often not stiff enough to constrain the mast base in a rigid manner. Several sensors are placed along the mast to measure acceleration signals of the mast, which are further used to evaluate the desirable control forces based on the control laws adopted.

3. Magneto-rheological dampers

3.1 Modelling of MR dampers

Magneto-rheological fluids have many attractive features, including high yield strength, low viscosity and stable hysteretic behaviour over a broad temperature range. MR dampers with a capacity of 20 tons have been designed and presumably tested by Carlson and Spencer (1996). Moreover, MR fluids can operate at temperatures ranging from -40°C to 150°C with only slight variations in the yield stress. Consequently, devices with MR fluids are expected to work well in installations on marine vessels.

To evaluate the potential of MR dampers in structural control applications and to take full advantage of the unique features of these devices, it is necessary to develop a model that can accurately reproduce the behaviour of MR dampers. Spencer *et al.* (1996) proposed a phenomenological model as shown in Fig. 3 to portray the behaviour of a prototype MR damper. This model is based on a Bouc-Wen hysteresis model and is governed by the following seven simultaneous equations:

$$f = c_1 \dot{y} + k_1(x - x_0) \quad (1)$$

$$\dot{y} = \frac{\alpha z + c_0 \dot{x} + k_0(x - y)}{c_0 + c_1} \quad (2)$$

$$z = (-\gamma)|\dot{x} - \dot{y}|z|z|^{\mu-1} - \beta(\dot{x} - \dot{y})|z|^\mu + A(\dot{x} - \dot{y}) \quad (3)$$

$$c_0 = c_{0a} + c_{0b}u \quad (4)$$

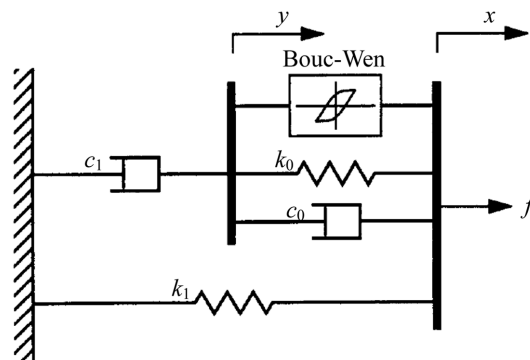


Fig. 3 Simple mechanical model of an MR damper

$$c_1 = c_{1a} + c_{1b}u \quad (5)$$

$$\alpha = \alpha_a + \alpha_b u \quad (6)$$

$$\dot{u} = -\eta(u - v) \quad (7)$$

where x is the displacement at the right end, f is the force generated, y is an internal pseudo displacement, u is the output of a first-order filter, and v is the commanded voltage sent to the current driver. In this model, k_1 is the accumulator stiffness; c_0 and c_1 are the viscous damping coefficients observed at high and low velocities, respectively; k_0 is introduced to control the stiffness at high velocities; x_0 is the initial displacement of spring k_1 associated with the nominal damper force due to the accumulator; γ , β , A , and μ are hysteresis parameters for the yield element; z is the evolutionary variable and α is the evolutionary coefficient. A total of 14 model parameters are used to characterize the prototype MR damper using experimental data. Yang *et al.* (2004) studied the 20-tons large-scale MR damper based on the Bouc-Wen hysteresis model, and confirmed the validity of this dynamic modelling.

The hysteretic behaviour of the damper is portrayed by the evolutionary variable z in Eq. (3). By adjusting the parameters γ , β , and A , the linearity in the unloading and the smoothness of the transient from the pre-yielding to the post-yielding regions can be controlled. Spencer (1986) showed that the upper limit of the evolutionary variable is

$$z_\mu = \left(\frac{A}{\gamma + \beta} \right)^{1/\mu} \quad (8)$$

In common cases of vibration control, the stiffness contributions in Eqs. (1) and (2) from the MR damper can be numerically shown to be small compared to the damping effects and hence is neglected in the following derivation. Substituting Eq. (8) into Eq. (2) and then Eq. (1), the upper bound of the damper force f_u can be approximated as

$$f_u \cong \frac{c_1}{c_0 + c_1} (\alpha z_\mu + c_0 \dot{x}) \quad (9)$$

Under rheological equilibrium and a constant voltage condition, the steady-state solution of the first-order filter represented by Eq. (7) is $u = v$. This steady-state solution can be substituted into Eqs. (4-6) and subsequently into Eq. (9), which results in the following expression

$$f_u \cong \frac{c_{1a} + c_{1b}u}{(c_{0a} + c_{1a}) + (c_{0b} + c_{1b})u} [(\alpha_a + \alpha_b u)z_\mu + (c_{0a} + c_{0b}u)\dot{x}] \quad (10)$$

Noting the typical maximum and minimum v values of 2.25 V and 0 V respectively, the maximum force F_{\max} and minimum force F_{\min} can be worked out accordingly.

3.2 Inverse neural network model

To carry out vibration control using MR dampers, it is essential to estimate the required voltage input to the MR damper so that a damper force as close to the optimal control force as possible can be produced. It is basically a nonlinear mapping between the inputs, namely the damper displacement, damper velocity and the perfect damper force estimated based on the control strategy adopted, and the output that is the required voltage input to the MR damper. The nonlinear mapping

can generally be written as

$$v = g(x, \dot{x}, f) \quad (11)$$

where v is the voltage required at time t , f is the perfect damper force, and x and \dot{x} are the damper displacement and velocity respectively.

A neural network model is used to simulate the nonlinear relationship expressed by Eq. (11). By trial and error, a neural network with two hidden layers is selected. The first hidden layer consists of 6 neurons while the second hidden layer comprises 20 neurons. The input data for the neural network are displacement, velocity and the optimal damper force while the output data is the required voltage. The required displacement and velocity data for training and testing the neural network are generated by superimposing a Gaussian white noise band limited between 0 Hz and 6 Hz on the displacement and velocity data obtained by solving the dynamic response of the ship mast under various excitations and the optimal control forces. The voltage is generated using uniformly distributed random numbers between 0 and 2.25. The damper force is generated by solving the phenomenological model represented by Eqs. (1-7). In the study, these data are sampled at 1/0.03 Hz for 105 s, resulting in 3500 sets of data. Out of these data, the first 1,500 data sets are used as training data while the remaining 2,000 data sets are used as testing data. These data are normalized before passing into the neural network for training and validating. As an example, the ship mast described in Section 7 is adopted and the control forces are determined by the classical optimal control algorithm. Part of the voltage time history of training and validation is shown in Fig. 4, which demonstrates that in general the voltage time history predicted by the neural network

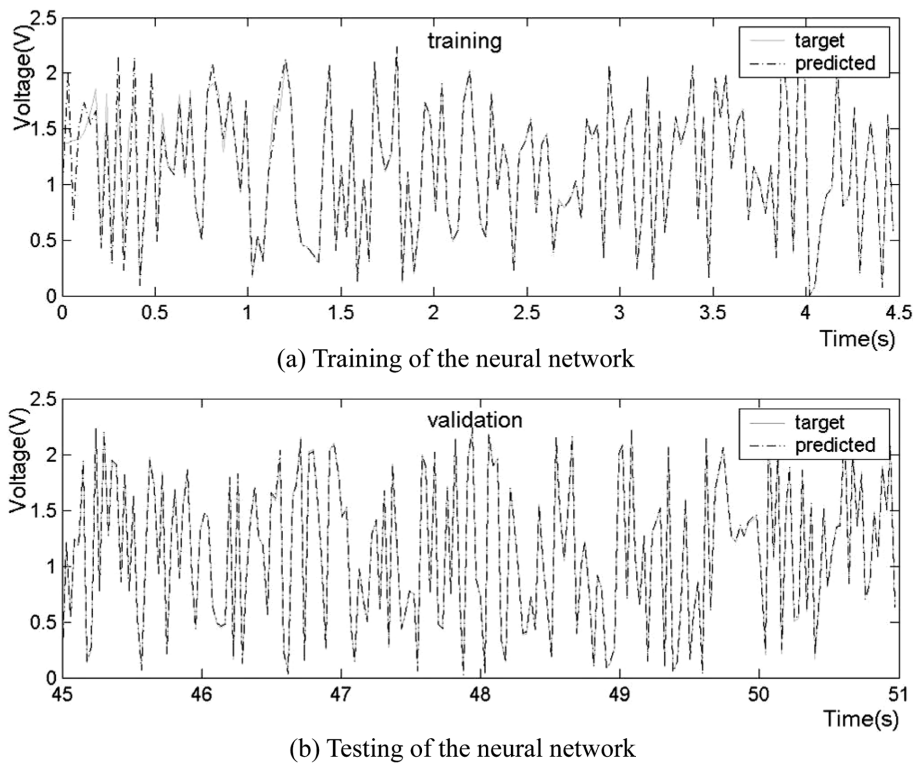


Fig. 4 Time histories of voltages at training and testing of the neural network

model follows the target voltage reasonably closely. The nearly perfect match indicates that the neural network model is well trained. It also illustrates that the inverse dynamic relationship of the prototype MR damper can be emulated by the neural network reasonably well.

4. Simulation of loading on the mast

4.1 Wind loading

Vibrations of the mast are elicited by the turbulent components of the wind. Wind turbulence in the atmospheric boundary layer is typified by random fluctuations of velocity and pressure. For structural design purposes, Davenport (1967) proposed the normalized one-sided power spectral density function of wind velocity

$$S_{v_i}(\omega_n) = 4Kv_{10}^2 \frac{x^2}{(\omega_n/2\pi)(1+x^2)^{4/3}} \quad (i = 1, 2, \dots, m; n = 0, 1, 2, \dots, N-1) \quad (12)$$

where K is a coefficient representing surface roughness, $x = 1200\omega_n/2\pi v_{10}$, ω_n is the frequency in rad/s and v_{10} is the wind speed at height 10 m in m/s. The normalized power spectral density of wind pressure is taken as

$$S_{w_i}(\omega_n) = \frac{4w_i^2}{v_i^2} S_{v_i}(\omega_n) \quad (13)$$

where $v_i = (h_i/10)^\alpha v_{10}$ is the wind speed at height h_i m and α is the roughness coefficient.

Taking the relationship between the wind velocity and pressure as $w_i = \rho v_i^2/2$, the wind load can be further expressed as

$$F_i(t) = W_i(t)A_i\mu_s\mu_r \quad (i = 1, 2, \dots, m) \quad (14)$$

where the shape coefficient μ_s is set to be 0.8 in the analysis, the recurrence interval coefficient μ_r is taken to be 1.2, A_i is the windward area, and the surface roughness coefficient K is set to be 0.003. As proposed by Shinozuka and Deodatis (1991), the wind pressure can be simulated by stochastic processes as

$$W_i(t) = \sqrt{2} \sum_{n=0}^{N-1} \sqrt{2S_{w_i}(\omega_n)\Delta\omega} \cdot \cos(\omega_n t + \varphi_n), \quad (n = 0, 1, 2, \dots, N-1) \quad (15)$$

where

$$\omega_n = n\Delta\omega, \quad (n = 0, 1, 2, \dots, N-1) \quad (16)$$

$$\Delta\omega = \omega_u/N \quad (17)$$

$$S_{w_i}(\omega_0)|_{\omega_0=0} = 0 \quad (18)$$

φ_n is an independent random phase angle, and N is a large number. Note that ω_u represents an upper cut-off frequency beyond which the power spectral density function $S_{w_i}(\omega_n)$ may be assumed to be zero for either mathematical or physical reason. As $\omega_u = N\Delta\omega$ is a fixed value, $\Delta\omega$ tends to zero when N approaches infinity. The following criterion is usually used to estimate the value of ω_u

$$\int_0^{\omega_u} S_{w_i}(\omega) d\omega = (1 - \varepsilon) \int_0^{\infty} S_{w_i}(\omega) d\omega \quad (19)$$

where ε ($\varepsilon \ll 1$) is a parameter that reflects the accuracy of using ω_u to replace the infinite upper limit. The independent random phase angles $\varphi_0, \varphi_1, \varphi_2, \dots, \varphi_{N-1}$ in Eq. (15) are distributed uniformly over the interval $[0, 2\pi]$. These random phase angles can be obtained by multiplying a random number distributed uniformly over the interval $[0, 1]$ by 2π .

The simulated stochastic process $W_i(t)$ given by Eq. (15) is periodic with a period of $T_0 = 2\pi/\Delta\omega$. This indicates that the smaller the value of $\Delta\omega$ is, or equivalently the larger N is under a specified upper cut-off frequency value ω_u , the longer the period of the simulated stochastic process is. Another very important point is that the simulated stochastic process $W_i(t)$ is asymptotically Gaussian as N approaches infinity because of the multi-variable central limit theorem.

At this point, it should be noted that when generating sample functions of the simulated stochastic process according to Eq. (15), the time step Δt separating the generated values of $W_i(t)$ in the time domain has to obey the condition

$$\Delta t \leq \pi / \omega_u \quad (20)$$

in order to avoid aliasing according to the sampling theorem as described by Bracewell (1999).

For the generation of sample functions of the stochastic process $W_i(t)$, an upper cut-off frequency ω_u must be specified. The value of $\omega_u = 88.468$ rad/sec is established by using the criterion described in Eq. (19) with $\varepsilon = 0.015$. If the parameter N is chosen to be 8192, then the other parameters are $\Delta\omega = \omega_u/N \cong 0.0108$ rad/sec and $T_0 = 2\pi/\Delta\omega = 581.77$ sec. To avoid aliasing, Eq. (20) also stipulates that $\Delta t \leq 0.0355$ sec. Fig. 5 shows a simulated time history of wind loading on the mast described in Section 7 at the node 27 m above the mast base.

4.2 Rolling

The ship rolling motion is assumed to be sinusoidal in the study. Fig. 6 depicts the rolling of the ship schematically as well as the inertial force and gravity force acting on the mast. The roll angle θ at time t can be expressed in terms of the rolling amplitude Θ and the rolling period T as

$$\theta = \Theta \sin(2\pi t/T) \quad (21)$$

The inertial force per unit length of the mast F_i can be written as

$$F_i = m(y_m)(y_m + y_{m0})\ddot{\theta} \quad (22)$$

where y_m is the distance above mast base and y_{m0} is the distance between the mast base and the axis

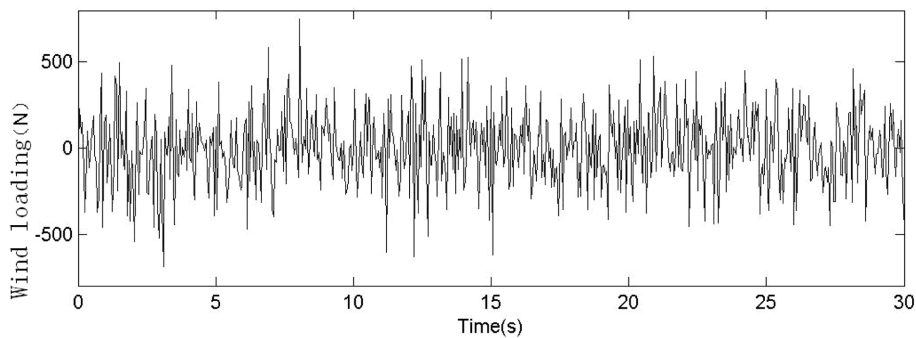


Fig. 5 Simulated time history of wind loading

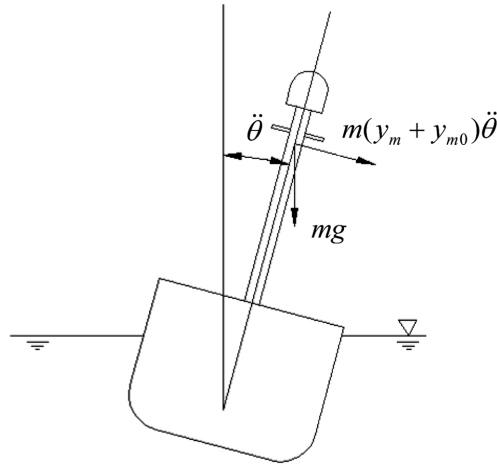


Fig. 6 Schematic diagram of the ship rolling

of rotation. Substituting the second derivative of the roll angle θ from Eq. (21) into Eq. (22), one gets another expression for the inertial force per unit length of the mast F_i as

$$F_i = -m(y_m)(y_m + y_{m0})(2\pi/T)^2 \Theta \sin(2\pi t/T) \tag{23}$$

The tangential component of gravity force at the roll angle θ is

$$G_i = m(y_m)g \sin \theta \tag{24}$$

Noting the roll angle θ given by Eq. (21) and that the sine of a small angle is approximately equal to the angle itself in radian, one has

$$G_i = m(y_m)g \Theta \sin(2\pi t/T) \tag{25}$$

Combining the inertial force and the tangential component of the gravity force, one can obtain the total loading perpendicular to the mast as

$$F = m(y_m)[-(y_m + y_{m0})(2\pi/T)^2 + g] \Theta \sin(2\pi t/T) \tag{26}$$

4.3 Base excitation

The mast is excited by the running propeller through ship hull girder vibrations. The vibration of the ship girder under the propeller excitations can be analyzed by the finite element method, and a typical computational model is shown in Fig. 7. Once the displacement time history of the node to which the mast base attaches is available, the acceleration at the mast base is obtained by repeated

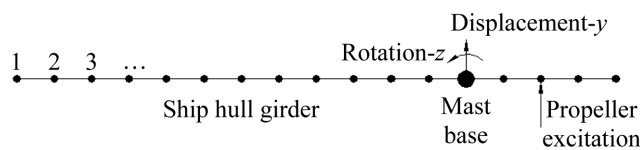


Fig. 7 Schematic diagram of computational model for base excitation

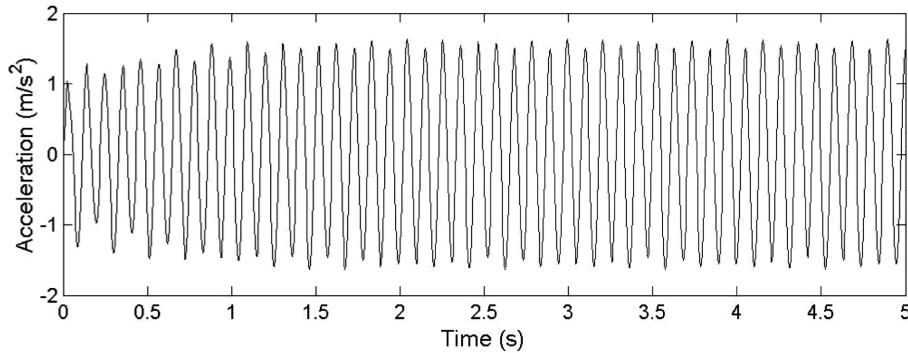


Fig. 8 Simulated time history of base excitation caused by the propeller

differentiation with respect to time. Fig. 8 depicts the acceleration time history at the mast base for a typical set of parameters for the propeller and the ship hull girder.

5. Control algorithms

The finite element method is employed in the analysis to obtain the dynamic response of the mast under wind loading, rolling, base excitation due to running propellers and control forces. The matrix equation of motion of the mast of dimension n under external loading and control forces can be written as

$$\mathbf{M}\ddot{\mathbf{X}} + \mathbf{C}\dot{\mathbf{X}} + \mathbf{K}\mathbf{X} = \mathbf{G}\mathbf{F}_e + \mathbf{H}\mathbf{F}_c \quad (27)$$

where \mathbf{X} , $\dot{\mathbf{X}}$ and $\ddot{\mathbf{X}}$ are the displacement, velocity and acceleration vectors respectively of dimension n , the over dot denotes differentiation with respect to time t , \mathbf{M} , \mathbf{C} and \mathbf{K} are the mass, damping and stiffness matrices of dimension $n \times n$, \mathbf{F}_e is the external load vector of dimension n , \mathbf{F}_c is the control force vector with dimension m , and \mathbf{G} and \mathbf{H} are the location matrices to apply the external loading and control forces to the appropriate nodes respectively, n is the total number of degrees of freedom of the mast, and m is the number of control devices. In the study, Rayleigh damping is assumed and therefore the damping matrix \mathbf{C} can be represented as

$$\mathbf{C} = \alpha_r \mathbf{M} + \beta_r \mathbf{K} \quad (28)$$

where the parameters α_r and β_r are normally obtained based on the first two sets of modal data.

The effectiveness of using the classical optimal control algorithm by Bryson and Ho (1975), the independent modal space control algorithm by Meirovitch (1985) and the fuzzy control algorithm by Mamdani (1974) for vibration control of the mast is then studied. It is assumed that the full state vector of the mast is available for control force calculation.

5.1 The classical optimal control algorithm

The state vector is defined as

$$\mathbf{Z} = \begin{bmatrix} \mathbf{X} \\ \dot{\mathbf{X}} \end{bmatrix} \quad (29)$$

The equation of motion of the mast under external excitation and control forces, namely Eq. (27), can therefore be further expressed in terms of the state vector as

$$\dot{\mathbf{Z}} = \mathbf{A}\mathbf{Z} + \mathbf{E}\mathbf{F}_e + \mathbf{B}\mathbf{F}_c \quad (30)$$

where

$$\mathbf{A} = \begin{bmatrix} \mathbf{0} & \mathbf{I} \\ -\mathbf{M}^{-1}\mathbf{K} & -\mathbf{M}^{-1}\mathbf{C} \end{bmatrix} \quad (31)$$

$$\mathbf{B} = \begin{bmatrix} \mathbf{0} \\ \mathbf{M}^{-1}\mathbf{H} \end{bmatrix} \quad (32)$$

$$\mathbf{E} = \begin{bmatrix} \mathbf{0} \\ \mathbf{M}^{-1}\mathbf{G} \end{bmatrix} \quad (33)$$

and $\mathbf{0}$ and \mathbf{I} are zero and identity matrices of dimension $n \times n$ respectively.

In order to obtain the optimal control force vector \mathbf{F}_c , a quadratic function of the state and control vectors is usually used, namely

$$J(t) = \frac{1}{2} \int_0^{\infty} (\mathbf{Z}^T \mathbf{Q} \mathbf{Z} + \mathbf{F}_c^T \mathbf{R} \mathbf{F}_c) dt \quad (34)$$

where \mathbf{Q} and \mathbf{R} are weighting matrices of the state and control forces respectively and they are usually symmetric. Minimization of Eq. (34) leads to the well known Riccati equation as follows

$$\mathbf{P}\mathbf{A} + \mathbf{A}^T \mathbf{P} - \mathbf{P}\mathbf{B}\mathbf{R}^{-1}\mathbf{B}^T \mathbf{P} + \mathbf{Q} = 0 \quad (35)$$

Once the Riccati matrix \mathbf{P} is available from Eq. (35), the optimal control force is given by

$$\mathbf{F}_c = -\mathbf{R}^{-1}\mathbf{B}^T \mathbf{P}\mathbf{Z} \quad (36)$$

In the study, the weighting matrices \mathbf{Q} and \mathbf{R} are set to be

$$\mathbf{Q} = r \begin{bmatrix} \mathbf{K} & \\ & \mathbf{M} \end{bmatrix} \quad (37)$$

$$\mathbf{R} = \mathbf{I} \quad (38)$$

where the parameter r is a weighting coefficient.

5.2 Independent modal space control algorithm

Introducing a transformation using the normalized mode shapes, the displacement vector \mathbf{X} can be written as

$$\mathbf{X} = \Phi \mathbf{q}(t) \quad (39)$$

where Φ is a matrix of dimension $n \times n$ containing the normalized mode shapes, and \mathbf{q} is the modal displacement vector. Eq. (27) can therefore be written in modal coordinates as

$$\ddot{\mathbf{q}} + \text{diag}[2\zeta_i \omega_i] \dot{\mathbf{q}} + \text{diag}[\omega_i^2] \mathbf{q} = \mathbf{U}_e + \mathbf{U}_c \quad (40)$$

where ζ_i is the modal damping parameter, ω_i is the eigenvalue, and the corresponding load vectors

in modal coordinates are

$$\mathbf{U}_e = \Phi^T \mathbf{G} \mathbf{F}_e \quad (41)$$

$$\mathbf{U}_c = \Phi^T \mathbf{G} \mathbf{F}_c \quad (42)$$

Eq. (40) actually represents n decoupled equations of motion in modal coordinates. Defining the state vector in modal coordinates \mathbf{w}_i as

$$\mathbf{w}_i = \begin{bmatrix} q_i \\ \dot{q}_i \end{bmatrix} \quad (43)$$

the i^{th} decoupled equations of motion in modal coordinates may be reformulated in the general state space form as

$$\dot{\mathbf{w}}_i = \mathbf{A}_i \mathbf{w}_i + \mathbf{E}_i U_{ei} + \mathbf{B}_i U_{ci} \quad (44)$$

where

$$\mathbf{A}_i = \begin{bmatrix} 0 & 1 \\ -\omega_i^2 & -2\zeta_i\omega_i \end{bmatrix} \quad (45)$$

$$\mathbf{B}_i = \begin{bmatrix} 0 \\ 1 \end{bmatrix} \quad (46)$$

$$\mathbf{E}_i = \begin{bmatrix} 0 \\ 1 \end{bmatrix} \quad (47)$$

and U_{ei} and U_{ci} are the i^{th} components of the vectors \mathbf{U}_e and \mathbf{U}_c respectively. The i^{th} modal control force is given by

$$F_i = -\mathbf{R}_i^{-1} \mathbf{B}_i^T \mathbf{P}_i \mathbf{w}_i \quad (48)$$

where the 2×2 Riccati matrix \mathbf{P}_i can be solved from the second-moment Riccati equation as follows

$$\mathbf{P}_i \mathbf{A}_i + \mathbf{A}_i^T \mathbf{P}_i - \mathbf{P}_i \mathbf{B}_i \mathbf{R}_i^{-1} \mathbf{B}_i^T \mathbf{P}_i + \mathbf{Q}_i = \mathbf{0} \quad (49)$$

5.3 Fuzzy control

The study employs a fuzzy control scheme with a fuzzy controller consisting of three modules, namely fuzzification, inference engine and defuzzification. The fuzzification module converts the scaled crisp values to fuzzy numbers with singleton membership functions. In this study, the implications of the fuzzy relations from “if-then” rules are realized by the method of Mamdani (1974), and triangular membership functions are used for various fuzzy numbers. In the inference engine module, approximate reasoning is conducted using the generalized *modus ponens*. In the module of defuzzification, the fuzzy control force is transformed into a crisp number by the appropriate methods such as the gravity centre approach.

In practice, measured inputs from a number of sensors, which may be in the form of crisp values, are converted into linguistic values or the fuzzy membership functions through the fuzzification process. The number of sensors used in the system is dependent on the number of input variables used in the controller. Membership functions can be of any shapes as long as they represent a mathematical function. Three of the most common are triangular, trapezoidal and Gaussian functions. The first step is to define the universe of discourse and to choose the appropriate input and output variables. The universe of discourse is a finite or infinite range of values which define the range of input or output values. In the study, the controller is designed to use two input

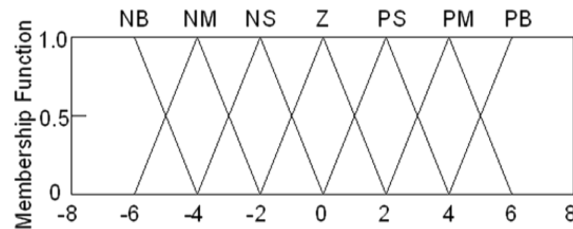


Fig. 9 Membership functions for the input and output variables

variables (i.e., displacement and velocity), and one output variable (i.e., control force). The input variables are first mapped to the interval $[-6, 6]$ with 13 discrete values. For each converted input variable, one may obtain 7 fuzzy linguistic values with different membership function values through 7 membership functions. The membership functions selected for the input variables for the analysis are of triangular shape as illustrated in Fig. 9. The 7 fuzzy linguistic values are: NB (Negative Big), NM (Negative Medium), NS (Negative Small), Z (Zero), PS (Positive Small), PM (Positive Medium) and PB (Positive Big). Similarly, one may obtain 7 fuzzy linguistic values with different membership function values for the output variable.

In general, the fuzzy logic controller uses fuzzy inference with rules based on engineering experience. Therefore it is essential to establish the control rule base required to achieve the control goal according to the experience and intuition of the experts. The more control rules there are in the rule base, the more effective the control is. Fuzzy inference is carried out using the fuzzy rule base developed, which performs various fuzzy logic operations to infer the control action for a given fuzzy input. Fuzzy rules are verbose sentences which define the way that the input linguistic variables are related to the output linguistic variables. The most widely used fuzzy rules are in the form of “if-then” statements. The heuristic inference rules based on the structural displacement and velocity are summarized in Table 1. Note that with two input variables and one output variable, the fuzzy rule base matrix consists of 49 rules. The fuzzy inference surface in Fig. 10 shows the nonlinear relationship between the input and output. The control chart shown in Table 2, which combines two inputs to form an output, is used in the fuzzy control system described in this paper.

The final stage of the fuzzy control is known as defuzzification in which the inferred fuzzy control action is converted into crisp control values required to implement real operational control. Many effective defuzzification strategies, such as the gravity centre approach and the scheme based on the maximum of the membership function, are available to obtain the output crisp values. In the

Table 1 Fuzzy inference rules

F_c		\dot{x}						
		NB	NM	NS	Z	PS	PM	PB
x	NB	PB	PB	PM	PM	PS	PS	Z
	NM	PB	PM	PM	PS	PS	Z	NS
	NS	PM	PM	PS	PS	Z	NS	NS
	Z	PM	PS	PS	Z	NS	NS	NM
	PS	PS	PS	Z	NS	NS	NM	NM
	PM	PS	Z	NS	NS	NM	NM	NB
	PB	Z	NS	NS	NM	NM	NB	NB

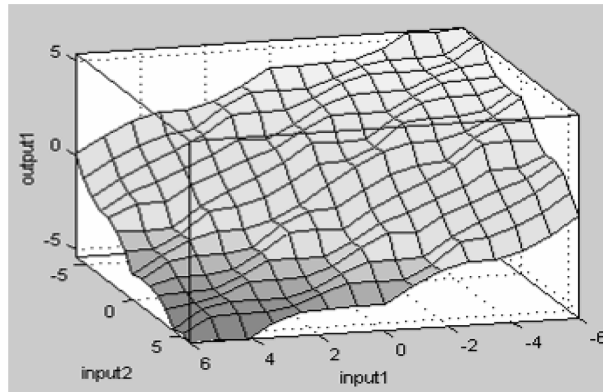


Fig. 10 Fuzzy inference surface

Table 2 Control chart used in fuzzy control system

F_c	\dot{x}													
	-6	-5	-4	-3	-2	-1	0	1	2	3	4	5	6	
-6	5.4	5.3	5.4	4.3	4.0	4.0	4.0	3.0	2.0	2.0	2.0	1.0	0.0	
-5	5.3	4.3	4.3	4.3	4.0	3.0	3.0	3.0	2.0	1.0	1.0	0.0	-1.0	
-4	5.4	4.3	4.0	4.0	4.0	3.0	2.0	2.0	2.0	1.0	0.0	-1.0	-2.0	
-3	4.3	4.3	4.0	3.0	3.0	3.0	2.0	1.0	1.0	0.0	-1.0	-1.0	-2.0	
-2	4.0	4.0	4.0	3.0	2.0	2.0	2.0	1.0	0.0	-1.0	-2.0	-2.0	-2.0	
-1	4.0	3.0	3.0	3.0	2.0	2.0	1.0	0.0	-1.0	-1.0	-2.0	-3.0	-3.0	
x 0	4.0	3.0	2.0	2.0	2.0	1.0	0.0	-1.0	-2.0	-2.0	-2.0	-3.0	-4.0	
1	3.0	3.0	2.0	1.0	1.0	0.0	-1.0	-2.0	-2.0	-3.0	-3.0	-3.0	-4.0	
2	2.0	2.0	2.0	1.0	0.0	-1.0	-2.0	-2.0	-2.0	-3.0	-4.0	-4.0	-4.0	
3	2.0	1.0	1.0	0.0	-1.0	-1.0	-2.0	-2.9	-2.9	-3.0	-4.0	-4.3	-4.3	
4	2.0	1.0	0.0	-1.0	-2.0	-2.0	-2.0	-3.0	-4.0	-4.0	-4.0	-4.3	-5.4	
5	1.0	0.0	-0.9	-1.0	-2.0	-3.0	-3.0	-3.0	-4.0	-4.3	-4.3	-4.3	-5.3	
6	0.0	-0.9	-1.9	-1.9	-2.0	-3.0	-3.9	-3.9	-4.0	-4.3	-5.3	-5.2	-5.4	

analysis, the inference conclusion obtained through fuzzification is defuzzified into the crisp values using the gravity centre approach.

6. Semi-active control system

The vibrations of the mast excited by wind, rolling and base excitation are controlled using MR dampers. Fig. 11 illustrates the proposed control strategy to realize the objectives. There is basically no restriction on the type of control algorithm to be used as long as it calculates a desirable control force based on the response data picked up by sensors. The desirable control force and the response of the mast are passed into an MR damper constraint filter. The filter will pass the control force and the corresponding displacement and velocity to the inverse neural network to estimate the voltage if the control force is within the maximum and minimum values that the MR damper can produce; otherwise the filter instructs the controller to feed the highest or lowest voltage to the MR damper

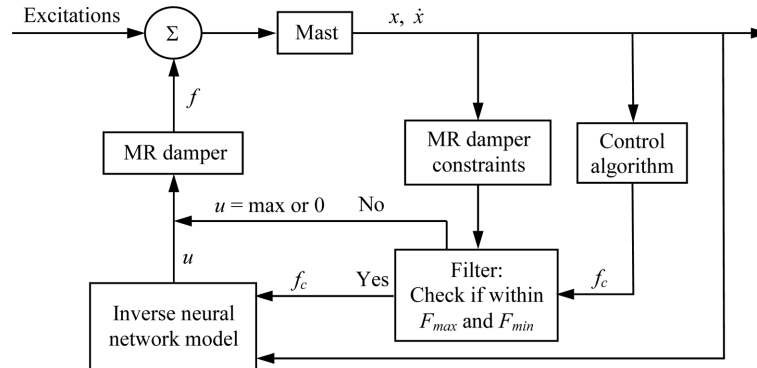


Fig. 11 Control block representation

directly depending on the control force being higher than the upper limit or less than the lower limit, respectively.

7. Numerical example

Consider a 30m tall uniform axi-symmetrical mast as shown in Fig. 1 guyed by two identical pairs of cables in the transverse and longitudinal planes. Each cable has one end connected to a stiff cross bar at the upper part of the mast and another end connected to one end of the shaft of an MR damper through a roller. The properties of the mast are as follows: total height $h=30$ m, flexural rigidity $EI=320$ MNm², mass per unit length $\rho A=142.6$ kg/m, height of cross bar from mast base $l=27$ m, distance between the mast base and the axis of rotation due to rolling $y_{m0}=12$ m, distance from tip of cross bar to centreline of mast $d=1$ m, and angle between guy cable and vertical $\psi=30^\circ$. The mast is modelled by 6 beam elements of length 3 m, 6 m, 6 m, 6 m, 6 m, and 3 m starting from the base. The stiff cross bar 27 m above the base is taken to be rigid in the analysis. Rayleigh damping with parameters $\alpha_r=0.16413$ and $\beta_r=0.001119$ is assumed. The mass of the radar is 500 kg. The rolling amplitude Θ is $\pi/12$ rad while the rolling period T is 8 s. The spring stiffnesses to model the imperfect fixity at the base of the mast are obtained from the finite element analysis of the plated panel structure of deck on which the mast is mounted.

The wind loading is assumed to be spatially fully uncorrelated and simulated as follows. The normalized one-sided power spectral density function of wind velocity is obtained from Eq. (12). The normalized power spectral density of wind pressure is calculated from Eq. (13). The wind pressure can be simulated by stochastic processes using Eq. (15). Eq. (14) then gives the wind load. The wind loads acting on the 6m long segments of the 30m tall mast are then evaluated and applied on the 5 intermediate nodes.

The simulation of vibration control comprises five modules, including those for finite element modelling, actuator modelling with neural network, external loading, control algorithm and dynamic structural response. The finite element model of the mast makes use of beam-column, mass and spring elements. The time history of external loading has been calculated in advance and saved as an array in the simulation system for subsequent application. The inverse neural network model is stored in the system as a series of coefficients and two kinds of transfer functions.

The classical optimal control (COC) algorithm, the independent modal space control (IMSC)

algorithm and the fuzzy control (FC) algorithm are employed to control the mast vibrations and their respective effectiveness is evaluated. The wind loading, inertial force caused by ship rolling and base excitation induced by the propeller are applied to the mast simultaneously. Wind loading acts horizontally, and three different directions of wind loading are considered, namely $\varphi=0^\circ$, 45° and 90° where φ is the angle between the wind direction and the transverse plane.

To evaluate the effectiveness of various algorithms in reducing the rotations of the radar at mast top, all rotations computed are normalized by the magnitude of maximum rotation without the MR damper. To demonstrate the advantage of using an MR damper in a semi-active control system, the case in which the MR damper acts as a passive damper with zero voltage input is also considered. Figs. 12-14 show the time histories of the normalized rotations of the mast top with the MR damper as in either semi-active or passive mode and without the MR damper. It is observed that the rotations of the mast top are significantly reduced by using the MR damper as a semi-active control device. However when it acts as a passive damper, the rotations are also reduced but not as

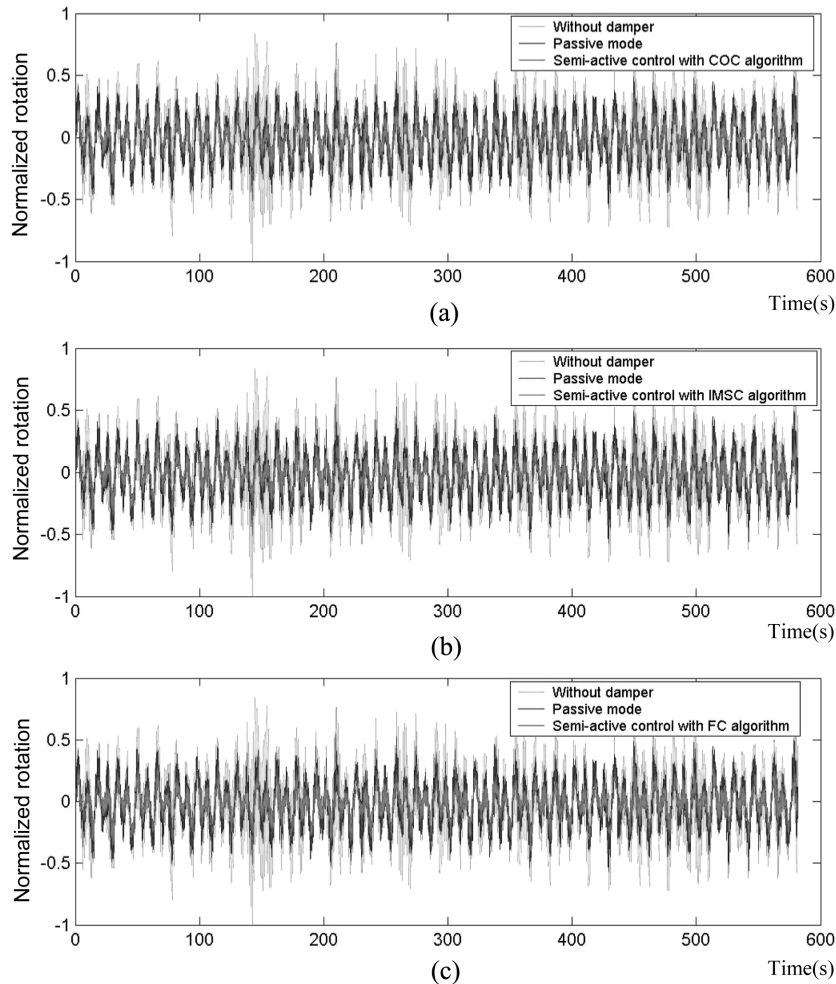


Fig. 12 Time histories of rotation at top of mast under different loading with MR damper used in semi-active or passive mode and without damper ($\varphi=0^\circ$)

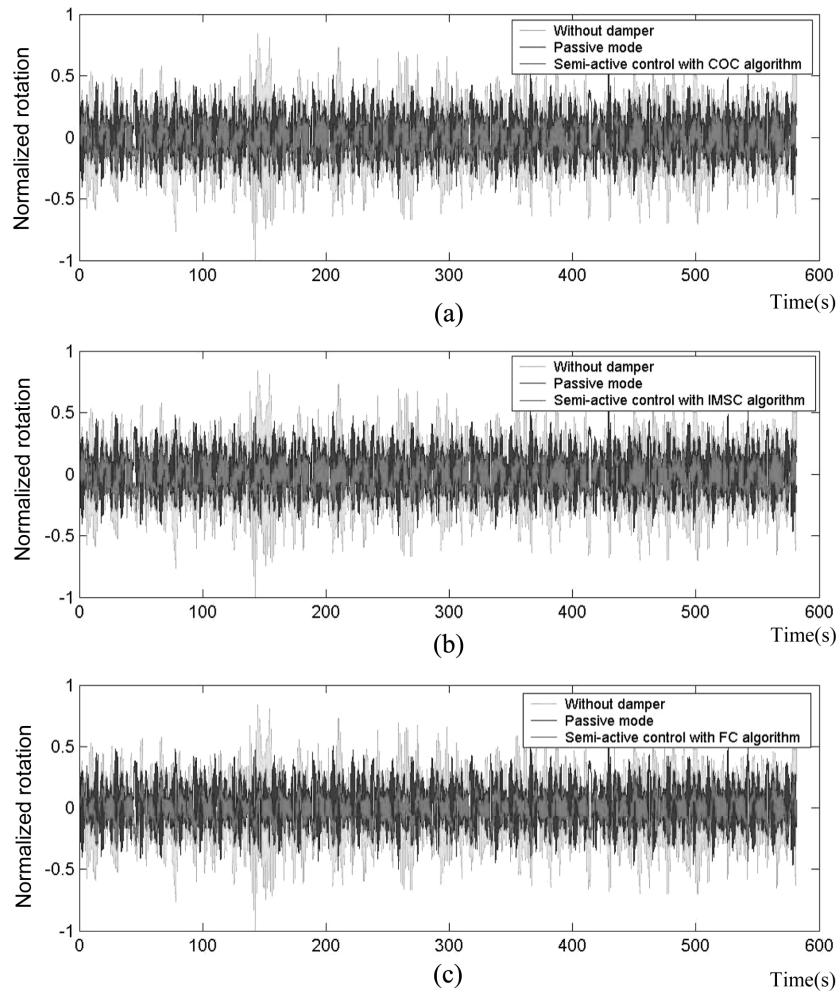


Fig. 13 Time histories of rotation at top of mast under different loading with MR damper used in semi-active or passive mode and without damper ($\varphi=45^\circ$)

significantly. The statistics of reduction in the peak and mean values of the normalized rotations are shown in Table 3. Generally speaking, the three control algorithms have similar control efficiencies. Both the COC and IMSC algorithms make use of the Riccati equation to determine the optimal control force. Comparatively the IMSC algorithm is more convenient than the COC algorithm as the computations required by the former are less complicated. However the fuzzy control algorithm is the most attractive among the three algorithms evaluated because it uses only the displacement and velocity of the position of the mast to which the guy cables with MR dampers are connected.

8. Conclusions

The application of MR dampers to vibration control of a ship mast subject to wind loading, ship rolling and base excitation simultaneously is studied. The classical optimal control algorithm, the

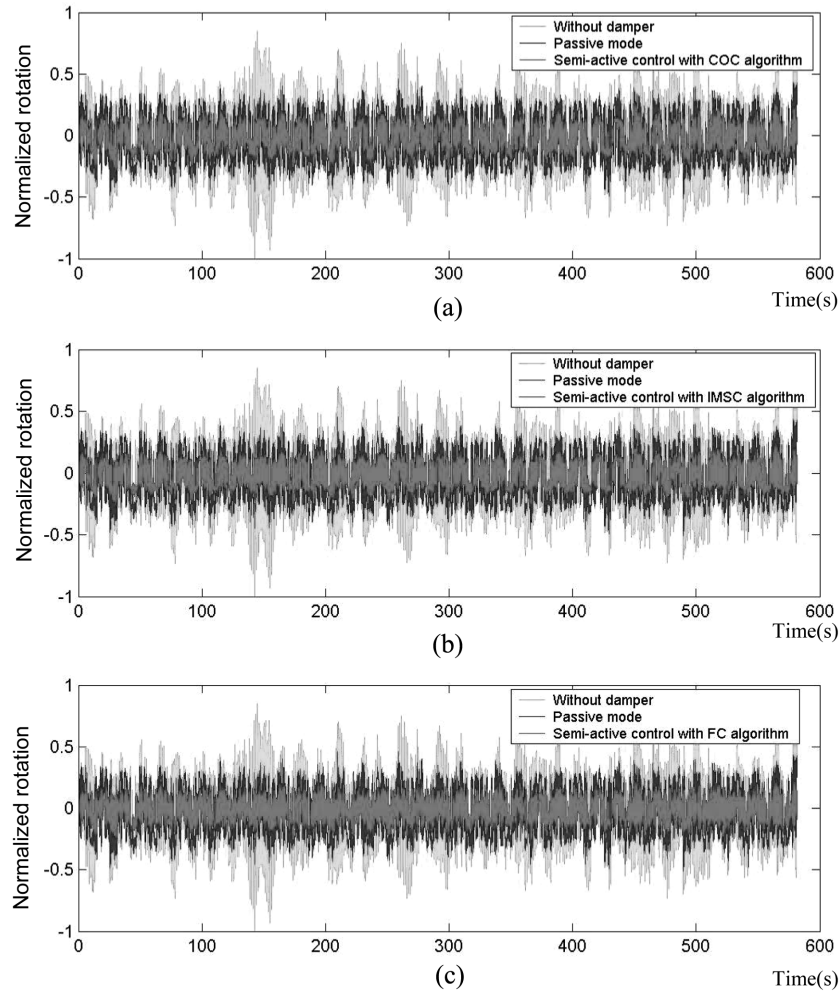


Fig. 14 Time histories of rotation at top of mast under different loading with MR damper used in semi-active or passive mode and without damper ($\varphi=90^\circ$)

Table 3 Reduction of normalized mast-top rotations

φ	COC algorithm		IMSC algorithm		FC algorithm		Passive mode	
	Peak	Mean	Peak	Mean	Peak	Mean	Peak	Mean
0°	55.4%	52.1%	55.7%	55.2%	53.6%	56.5%	43.1%	23.7%
45°	62.5%	57.5%	64.0%	58.7%	64.8%	63.9%	45.0%	27.4%
90°	64.5%	62.9%	68.2%	63.6%	69.2%	64.3%	49.1%	25.5%

independent modal space control algorithm and the fuzzy control algorithm are respectively examined in the study to carry out vibration control. The back-propagation neural network is also capable of emulating the inverse dynamic characteristics of MR dampers. Numerical simulations show that all three control algorithms combined with the force-output characteristics of the MR damper can effectively suppress the rotational vibrations at the top of mast and generally speaking

they have similar control efficiencies. From the practical point of view of control feasibility, the fuzzy control algorithm is the most attractive as less input is required and the computation is less intensive. The MR damper as used in a semi-active control system is therefore a reliable device with low power consumption.

Acknowledgements

The work described in this paper has been substantially supported by the National Natural Science Foundation of China (Project No. 50479050) and the Committee on Research and Conference Grants, The University of Hong Kong, Hong Kong, China.

References

- Bracewell, R.N. (1999), "The Fourier Transform and its Applications", McGraw-Hill.
- Bryson, A.E. and Ho, Y.C. (1975), "Applied optimal control: optimization, estimation and control", Washington, D.C: Hemisphere Publishing Corporation.
- Carlson, J.D. and Spencer, Jr., B.F. (1996), "Magneto-rheological fluid dampers for semi-active seismic control", *Proceeding of 3rd International Conference on Motion and Vibration Control*. Chiba, Japan, September, III, 35-40.
- Chang, C.C. and Roschke, P. (1999), "Neural network modeling of a magnetorheological damper", *J. Intel. Mater. Syst. Struct.*, **9**(9), 755-764.
- Chang, C.C. and Zhou, L. (2002), "Neural network emulation of inverse dynamics for a magnetorheological damper", *J. Struct. Eng.*, **128**(2), 231-239.
- Davenport, A.G. (1967), "Gust loading factors", *J. Struct. Div.*, **93**(ST3), 11-34.
- Dyke, S.J., Spencer, Jr., B.F., Sain, M.K., and Carlson, J.D. (1996), "Modeling and control of magnetorheological dampers for seismic response reduction", *Smart Mater. Struct.*, **5**, 565-575.
- Housner, G.W., Bergman, L.A., Caugher, T.K., Chassiakos, A.G., Claus, R.O., Masri, S.F., Skelton, R.E., Soong, T.T., Spencer, B.F., and Yao, J.T.P. (1997), "Structural control: past, present, and future", *J. Eng. Mech.*, **123**(9), 897-971.
- Hsueh, W.J. and Lee, Y.J. (1992), "Active vibration control on the mast of warships", *Int. Shipbuild. Prog.*, **39**(417), 79-94.
- Jansen, L.M. and Dyke, S.J. (2000), "Semiactive control strategies for MR dampers: Comparative study", *J. Eng. Mech.*, **126**(8), 795-803.
- Jung, H.J., Spencer, Jr., B.F., and Lee, I.W. (2003), "Control of seismically excited cable-stayed bridge employing magnetorheological fluid dampers", *J. Struct. Eng.*, **129**(7), 873-883.
- Mamdani, E.H. (1974), "Application of fuzzy algorithms for control of simple dynamic plant", *Pro. Inst. Elect. Eng.*, **121**(12), 1585-1588.
- Meirovitch, L. (1985), *Introduction to Dynamics and Control*, New York: Wiley.
- Mohammed, A., Kenny, C.S. and Kwok, F.N. (2004), "Active control of cross wind response of 76-story tall building using a fuzzy controller", *Eng. Struct.*, **130**(4), 492-498.
- Shinozuka, M. and Deodatis, G. (1991), "Simulation of stochastic process by spectral representation", *Appl. Mech. Rev.*, **44**(4), 191-203.
- Spencer, Jr., B.F., Dyke, S.J., Sain, M.K., and Carlson, J.D. (1996), "Phenomenological model for magnetorheological dampers", *J. Eng. Mech.*, **123**(3), 230-237.
- Spencer, Jr., B.F. (1986), *Reliability of Randomly Excited Hysteretic Structures*. New York, Springer-Verlag.
- Wang, J.Y., Ni, Y.Q., Ko, J.M., and Spencer, Jr., B.F. (2005), "Magneto-rheological tuned liquid column dampers (MR-TLCDs) for vibration mitigation of tall buildings: Modelling and analysis of open-loop control source", *Comput. Struct.*, **83**(25-26), 2023-2034.

- Xu, Y.L., Qu, W.L., and Ko, J.M. (2000), "Seismic response control of frame structures using magnetorheological/electrorheological dampers", *Earthq. Eng. Struct. D*, **29**, 557-575.
- Yang, G.Q., Spencer, Jr., B.F., Jung, H.J., and Carloson, J.D. (2004), "Dynamic modeling of large-scale magnetorheological damper systems for civil engineering applications", *J. Eng. Mech.*, **130**(9), 1107-1114.
- Zhu, W.Q., Luo, M., and Dong, L. (2004), "Semi-active control of wind excited building structures using MR/ER dampers", *Prob. Eng. Mech.*, **19**(3), 279-285.